Mask R-CNN Applied to Quasi-particle Segmentation from the Hybrid Pelletized Sinter (HPS) Process

Natália F. De C. Meira[1][a], Mateus C. Silva[2][b], Andrea G. C. Bianchi[2][c], Cláudio B. Vieira[1], Alinne Souza[3], Efrem Ribeiro[3], Roberto O. Junior[3] and Ricardo A. R. Oliveira[2][d]

[1]*Metallurgical Engineering Department, Federal University of Ouro Preto, Ouro Preto, Brazil*

[2]*Department of Computer Science, Federal University of Ouro Preto, Ouro Preto, Brazil*

[3]*ArcelorMittal, João Monlevade, Brazil*

Keywords: Convolutional Neural Network, Segmentation, Mask R-CNN, Steel Industry.

Abstract: Particle size is an important quality parameter for raw materials in steel industry processes. In this work, we propose to implement the Mask-R-CNN algorithm to segment quasi-particles by size classes. We created a dataset with real images of an industrial environment, labeled the quasi-particles by size classes, and performed four training sessions by adjusting the model's hyperparameters. The results indicated that the model segments with well-defined edges and applications as classes correctly. We obtained a mAP between 0.2333 and 0.2585. Additionally, hit and detection rates increase for larger particle size classes.

1 INTRODUCTION

The advent of deep learning models strengthened the development of works in the areas of object recognition and detection and classification, with superior results compared to conventional machine learning techniques (LeCun et al., 2015). Another advantage is the generalization to problems involving complex images as they learn how to extract more abstract features.

Some of the limitations are that these models are computationally intensive and require a large volume of data for training. Within the scope of data preparation, a complex problem to solve is labeling the data. This process is an expensive operation that often requires an expert to do it manually, which can be exhausting. Additionally, images with small objects are potentially challenging. The challenge of segmenting small objects in images tends to increase when many objects of interest are in the scene.

[a] https://orcid.org/0000-0002-7331-6263

[b] https://orcid.org/0000-0003-3717-1906

[c] https://orcid.org/0000-0001-7949-1188

[d] https://orcid.org/0000-0001-5167-1523

Thus, these applications increasingly aim to solve different problems, including the industrial scope in some cases. One of these problems is the detection of small particle sizes in a scene. Obtaining particle size by imaging methods can significantly contribute to process improvement.

Obtaining particle size from images is a challenging problem. The initial issue is because, in many contexts, these particles are small. Also, the image characteristics are affected: (i) by image resolution and noise; (ii) variations in ambient lighting; (iii) the density of objects that produce complex background; (iv) overlapping and occlusion of objects, and; (v) homogeneity in the particles' shape, color, and texture.

There is a non-conventional sintering process in the steel industry plants known as the Hybrid Pelletized Sinter (HPS) process. This stage produces micro-agglomerates of raw materials (iron ore, fuels, and fluxes) known as quasi-particles. Controlling the size of micro-agglomerates is essential, as it is the main characteristic that affects the permeability of the sintering furnace and, consequently, the productivity of the process. The particle size distribution of the quasi-particles is performed manually by an operator using the conventional sieving method several times a day.

Meira, N., Silva, M., Bianchi, A., Vieira, C., Souza, A., Ribeiro, E., O. Junior, R. and Oliveira, R.
Mask R-CNN Applied to Quasi-particle Segmentation from the Hybrid Pelletized Sinter (HPS) Process.
DOI: 10.5220/0010836900003124
In *Proceedings of the 17th International Joint Conference on Computer Vision, Imaging and Computer Graphics Theory and Applications (VISIGRAPP 2022) - Volume 4: VISAPP*, pages 462-469
ISBN: 978-989-758-555-5; ISSN: 2184-4321

In this work, we propose the segmentation of quasi-particles by size classes through images. The implementation uses the Mask R-CNN algorithm, known as the most influential instance segmentation structure. Thus, from an image obtained with the sample of micro-clusters, the algorithm segments the edges and assigns the size class. Thus, the main contribution of our work is:

- An implementation to obtain the size classes of micro-clusters from a dataset elaborated with systematically labeled industrial data.

This work is organized as follows: Section 2 presents the literature review, Section 3 presents related works, Section 4 presents the methodology used, from the elaboration of the dataset to its labeling, training hyperparameters, and metrics. In the evaluation, Section 5 presents the results obtained in the segmentation of microclusters and in Section 6 the Conclusion.

2 THEORETICAL BACKGROUND

This section presents the theoretical background applied in the context of this work. Here, we present the features and architecture of the Mask R-CNN model, used in this implementation.

2.1 Mask R-CNN

The computer vision community, driven by baseline systems such as Fast and Faster RCNN (Girshick, 2015; Ren et al., 2015) and Fully Convolutional Network (FCN) (Long et al., 2015), advanced in the detection and semantic segmentation tasks of objects. The semantic segmentation task is a challenging task, as it requires the correct detection of objects in the image and precisely segmenting each instance (He et al., 2017).

Semantic segmentation combines classic computer vision tasks: detecting objects individually, locating with a bounding box, and performing semantic segmentation, in which each pixel is classified into a set of categories without differentiating object instances (He et al., 2017). Thus, He et al. (He et al., 2017) proposed the Mask R-CNN method, which extends the Faster R-CNN to predict segmentation masks in each region of interest (Rol Align – RoI) with a parallel branch for classification and bounding box regression.

An advance on the work of He et al. (He et al., 2017) was the impact of RoI, which improved mask accuracy from 10% to 50%, and gains by decoupling mask and class prediction, so that RoI could predict category individually without class competition. This advance is mainly due to the contrast caused by the FCNs, which combined segmentation and classification, which did not work for instance segmentation.

Mask R-CNN's network architecture was instantiated in several architectures, divided into: (i) convolutional backbone architecture for resource extraction from an entire image and (ii) network head for bounding box recognition (classification and regression) and mask prediction applied individually to each RoI. For the backbone architecture, the ResNet (He et al., 2016) and ResNeXt (Xie et al., 2017) networks were evaluated, with depths of 50 or 101 layers. For the head of the network, Mask R-CNN added a fully convolutional mask prediction branch (He et al., 2017).

3 RELATED WORK

Works with challenging problems seek to implement the Mask R-CNN, mainly for small objects, which set the Mask R-CNN as the most influential instance segmentation structure according to (Zhang et al., 2020). De Césaro Júnior and Rieder (De Cesaro Júnior et al., 2020) proposed a routine for counting and automatically identifying insects in images. For the authors, the manual task of counting and identifying small insects is an exhaustive task, and the implementation of the Mask R-CNN had as a preliminary result a mAP of 60.4%.

The work by Cohn et al. (Cohn et al., 2021) implemented the Mask R-CNN for image analysis of gas-atomized nickel superalloy metallic powder particles with potential application in additive manufacturing. The authors obtained the images by Scanning Electron Microscopy (SEM), and after training with the Mask R-CNN, the masks showed good agreement with the dust particles present in the image. The achieved precision was 0.938 and the recall 0.799.

Chen et al. (Chen et al., 2020) implemented the Mask R-CNN in metallographic images for the segmentation of an aluminum alloy microstructure. As a contribution of the article, the authors suggested that the implementation can perform the segmentation of instances of microstructures in metallographic images of aluminum alloys automatically, providing a more effective tool for analyzing these images.

Other works showed the generalization of the implementation of the Mask R-CNN and its improvement for the automatic detection of animals (Tu et al., 2021; Bello et al., 2021; Xu et al., 2020), detection of aircraft and buildings in images remote sensing and satellite images (Wu et al., 2021; Zhang et al., 2019; Zhao et al., 2018), medical imaging, for example, for the segmentation of nuclei and tumors, cell nuclei and nodules pulmonary (Vuola et al., 2019; Zhang et al., 2019; Johnson, 2018),maintenance and control of manufacturing processes (Xi et al., 2020) and mapping, quantization and particle size distribution of clasts (Soloy et al., 2020).

Due to the generalization of the Mask R-CNN for several problems of different nature, and the need to individualize the quasi-particles, we implemented the Mask R-CNN for the problem presented in this work.

4 METHODOLOGY

In this section, we present the methodology implemented for the segmentation of quasi-particles. We describe dataset design, hyperparameter adjustment, training, and assessment metrics.

4.1 Dataset

We elaborated the datasets with images from real samples of quasi-particles, obtained in the industrial environment. After sampling in a tray with the assistance of an operator, the particles were photographed on the tray and sieved. The particles from each sieve were placed again in trays and photographed. Thus, each image had particles with a known particle size range. We consider these size ranges as classes for segmentation in the Mask R-CNN algorithm.

The classes were named according to the particle size range in millimeters: '2-3', 3-4', '4-6', '8-9' and '>9', totaling 5 classes. The Mask R-CNN algorithm considers the image background as a class, totaling 6 classes for training.

To carry out the training using the Mask R-CNN modifying the hyperparameters, we created a dataset containing 81 images for training, with 4801 annotated regions (labeled) and 46 images for validation, containing 460 annotations (Table 1). Images were resized to 1488x1488x3 before annotation to accommodate available hardware capacity.

Table 1: Number of images and annotations in the dataset.

	Number of images	Annotated regions
Training	81	4801
Validation	46	460

We perform the annotations manually using the VIA tool (VGG Image Annotator), which is an open-source project developed by the Visual Geometry Group (VGG) for manual annotation.

4.2 Hyperparameters

We implemented the Mask R-CNN[1] from the original repository available on GitHub. We adjusted some hyperparameters to reconcile with the model proposed in this study, based on the explanations of De Cesaro Júnior (De Cesaro Júnior et al., 2020). The first hyperparameter consists of the backbone, convnet architecture of the first stage of Mask R-CNN.

The training used the two backbones, ResNet50 and ResNet101, to compare the differences in training time and precision. We performed all training with the same dataset presented in the previous section to compare only the results and adjustments of the hyperparameters.

We implement it with the standard values of learning rate and weight decay, with values of 0.001 and 0.0001, respectively.

The hyperparameters adjusted in each training are in Table 2. The backbone is the ConvNet architecture used in the first stage of Mask R-CNN. TRAIN_ROIS_PER_IMAGE is the maximum number of ROI's (Region of Interest) that the RPN will generate for the image. MAX_GT_INSTANCES is the number of instances that can be detected in an image. DETECTION_MIN_CONFIDENCE is the confidence threshold beyond which classification of an instance will occur.

The IMAGE_MIN_DIM and IMAGE_MAX_DIM hyperparameters control the input resolution of the image which, by default, is resized to 1024x1024 sizes. In addition to these hyperparameters, the weights were initialized to the standard value of 1.

4.3 Training

We performed 4 training sessions, and for transfer learning, we used the weights from the MS COCO set. The trainings were carried out with 50 epochs and 100 epochs, and 100 steps per epoch.

We carry out the implementation in the Python programming language. We use the OpenCV library for image resizing and the Tensorflow and Keras libraries for training.

The hardware available for training was a computer with an Intel Core I7-6950X processor, 32 GB of RAM, and the GTX2080 graphics processing unit (GPU) with 8 GB of VRAM.

[1] https://github.com/matterport/Mask_RCNN

Table 2: Hyperparameter values adjusted in Mask R-CNN training for quasi-particles. The TRAIN columns symbolize each of the training.

HYPERPARAMETERS	TRAIN 1	TRAIN 2	TRAIN 3	TRAIN 4
BACKBONE	ResNet101	ResNet50	ResNet101	ResNet50
TRAIN_ROIS_PER_IMAGE	500	500	500	500
MAX_GT_INSTANCES	300	300	300	300
DETECTION_MAX_INSTANCES	500	500	500	500
DETECTION_MIN_CONFIDENCE	0.7	0.7	0.7	0.7
IMAGE_MIN_DIM	800	800	800	800
IMAGE_MAX_DIM	1024	1024	1024	1024
EPOCHS	50	50	100	100

4.4 Evaluation Criteria

For the graphical visualization of model losses, we use Tensorboard. The loss of Mask R-CNN is calculated according to Equation 1. In defined multitasking loss, Lcls is rank loss, Lbox is bounding box loss, and Lmask is mask loss (He et al., 2017).

$$L = L_{cls} + L_{box} + L_{mask} \tag{1}$$

To assess the precision of the model, we used the mAP metric, which is a metric often used in object recognition tasks. During detection, we seek to predict bounding boxes that overlap the labeled fundamental truth.

We can predict how good this overlap is by dividing the area of the overlap by the total area of both bounding boxes, giving the IoU (Intersection over Union) metric as shown in Equation 2. It is common for datasets to predefine an IoU threshold of 0.5 when sorting whether the prediction is a true positive or a false positive.

$$IoU = \frac{Area\ of\ Intersection}{Area\ of\ Union} = \frac{A \cap B}{A \cup B} \tag{2}$$

In image detection, precision refers to the percentage of bounding boxes predicted correctly (IoU > 0.5) about all bounding boxes predicted in the image, while recall is the percentage of bounding boxes predicted correctly (IoU > 0.5) of all objects in the image.

The IoU metric is the threshold for a correct prediction. Thus, we can plot a precision versus recall curve by the 0.5 IoU limit. This representation provides a curve with zigzag behavior for detection models, although it may vary for other models.

We then maximized the recall value for each precision value to smooth the curve's behavior. The area below the curve gives the average precision value, that is, the average precision, metric AP (Average Precision). The average of the AP metric across all images in a dataset gives the mAP metric (Mean Average Precision). We use the mAP metric to evaluate the model against the labeled validation dataset.

5 RESULTS

In this section, we present the results obtained with the implementation of the segmentation model. Preliminary results indicated that instance segmentation is an adequate approach for quasi-particle individualization and separation by size classes. Next, we describe the results of the segmentation masks, classes, evaluation metrics, and histograms generated by the Tensorboard.

5.1 Segmentation

We performed the training with the adjusted hyperparameters, shown in Section 3.2. The results showed that the segmentation masks converged with the edges of the quasi-particles and with the segmented instances separately, highlighting the class and the confidence of the class, as shown in Figure 1. The edges were well defined, especially for the larger particles.

The models were also accurate in avoiding the detection and segmentation of occluded and overlapping particles, a factor that could lead to errors incorrectly identifying the class.

5.2 Tensorboard

We visualize the values of training and validation losses with the help of the Tensorboard tool. In the graphs, the x-axis represents the number of training epochs and the y-axis represents the loss values. The loss values obtained by Mask RCNN are shown in Table 3.

The training loss values were between 0.5663 and 0.7702, in which the smallest loss was recorded in training 3, with the ResNet101 backbone and 100

Figure 1: The prediction correctly demonstrates the masks as instances of the same class, the bounding box, and the predicted confidence results. The image was taken from training 3.

Table 3: Loss values obtained in the 4 training sessions performed. The highlighted values represent the lowest value for the selected loss.

LOSSES	TRAIN 1	TRAIN 2	TRAIN 3	TRAIN 4
	50 epoch	50 epoch	100 epoch	100 epoch
loss	0.7702	0.7541	**0.5663**	0.5728
mrcnn_bbox_loss	0.06478	0.06426	**0.031**	0.03347
mrcnn_class_loss	0.1252	0.1221	0.077	**0.0768**
mrcnn_mask_loss	0.1567	0.1616	**0.1215**	0.1267
rpn_bbox_loss	0.3335	0.3062	0.2627	**0.259**
rpn_class_loss	0.08497	0.08507	**0.07416**	0.0768
val_loss	0.8825	0.8783	0.8222	**0.7977**
val_mrcnn_bbox_loss	0.1002	0.1001	0.0879	**0.08419**
val_mrcnn_class_loss	**0.1121**	0.1259	0.1646	0.1446
val_mrcnn_mask_loss	0.1657	0.1649	0.1684	**0.1641**
val_rpn_bbox_loss	0.3875	0.3715	**0.2952**	0.3012
val_rpn_class_loss	0.1168	0.1159	0.1061	**0.1035**

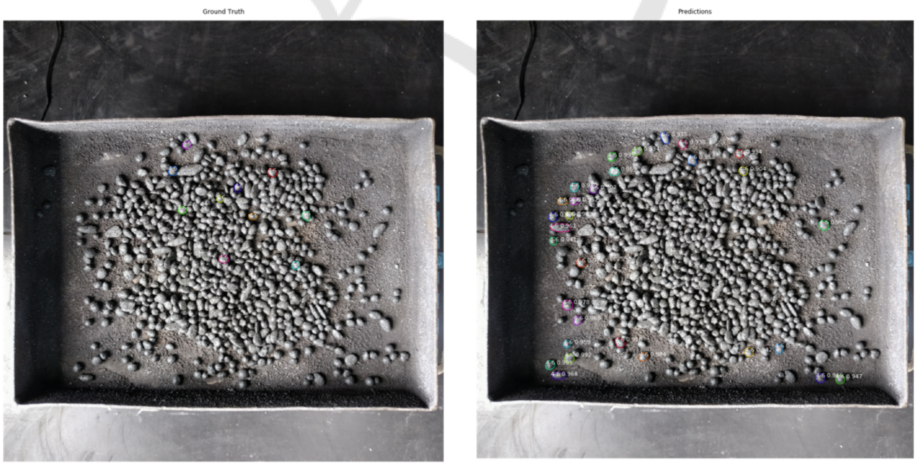

(a) (b)

Figure 2: Example of an image containing particles of class 4-6' from training 1. In a) the highlighted particles represent the particles labeled and calculated as ground truth, and in b) the highlighted particles represent the particles found by the model in predictions.

(a) (b)

Figure 3: An example image of particles of class '8-9' from training 4. In a) the highlighted particles as particles labeled and calculated as ground truth, and in b) the highlighted particles represent the particles found by the model in the prediction.

training epochs. Losses for detection by bounding boxes, generation of masks, and classification were quite positive, with the greatest loss for bounding boxes in the RPN refinement step. The graphics on the tensorboard were smooth for losses.

The graphs generated on the Tensorboard for the loss values for the validation showed fluctuations, mainly in the prediction of the classes in the validation. This behavior can be associated with the small number of labeling per image and the learning rate. Thus, the suggestions for improving this validation fluctuation behavior are annotation of a greater amount of images and objects per image and a decrease in the learning rate during training.

The overall validation loss values were between 0.7977 and 0.8825. Training 2 recorded the least loss, with the ResNet101 backbone and 100 training epochs.

Table 4 shows the time of each training according to the number of epochs. The number of epochs was decisive in the execution time of the training time, while the number of layers initialized by the Mask R-CNN backbone had no significant impact. Compared with the general loss values "loss" for training and "val loss" for validation, there was a decrease in loss with the increase in the number of times trained, with a single counterpart of the increase in model execution time.

We obtained the general loss values for training (loss) and validation (val loss) in the graphs generated by the Tensorboard, in Figures 4 and 5. The training graphs demonstrate a smooth descent to model convergence. We did not observe the same behavior in the validation step loss graphs, with constant fluctuations and increase after a certain number of epochs.

Table 4: Training execution time according to the backbone and number of epochs selected.

training	backbone	epochs	time to execution
TRAIN 1	ResNet101	50	1h 33m 29s
TRAIN 2	ResNet50	50	1h 33m 7s
TRAIN 3	ResNet101	100	3h 9m 13s
TRAIN 4	ResNet50	100	3h 9m 29s

5.3 Model Performance

To assess the performance of the model, we use the mAP metric with an IoU of 0.5. We obtained the ones for the 46 images in the validation set. The values obtained in each training are in Table 5.

Table 5: mAP metric values obtained for each training.

training	backbone	epochs	mAP
TRAIN 1	ResNet101	50	0.2334
TRAIN 2	ResNet50	50	0.2585
TRAIN 3	ResNet101	100	0.2333
TRAIN 4	ResNet50	100	0.2511

The mAP metric values were close for all training, and training 2 with ResNet50 and 50 epochs had the highest value. However, there was a discrepancy that impacted the mAP values. Images containing smaller particles, from the first three size classes, contained much more particles (objects per image) than images with larger particles, as the representations followed the sampling: for each sample containing 1Kg of material, proportionally, there are fewer particles of particle size greater than 6mm.

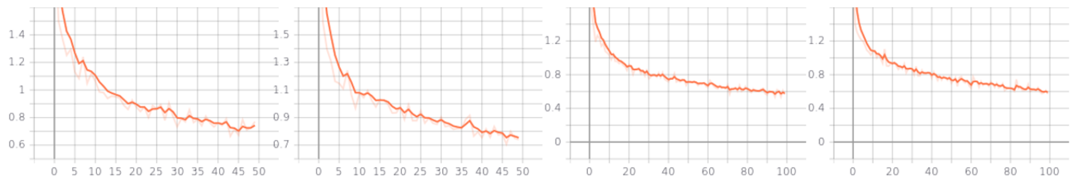

(a) (b) (c) (d)

Figure 4: The graphs represent the overall training loss: a) training 1; b) training 2; c) training 3, and; d) training 4.

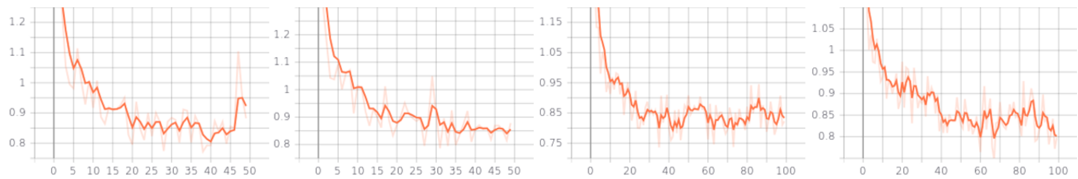

(a) (b) (c) (d)

Figure 5: The graphs represent the general loss of validation: a) training 1; b) training 2; c) training 3, and; d) training 4.

Thus, with only ten annotations on each image in the validation set, even though the model predicted many more particles than annotated, the mAP of these images were very small values. An example can be seen in Figure 2, where the prediction predicted many more particles than those labeled as ground truth.

The image in Figure 2 reached an AP of only 0.003 for an IoU of 0.5, showing the practical result of this discrepancy as shown in Figure 6.

For the cases of images containing larger particles, such as those of the '>9' class, the AP values per image were higher, reaching 90% for some images. This is because almost all particles in the image were labeled, so the chance of being contained in the prediction was also greater (Figure 3).

Figure 7 shows the result of the AP metric in Figure 3 on the precision-recall curve, with AP value equal to 0.551, that is, AP50= 55.1%, revealing the discrepancy with Figure 6.

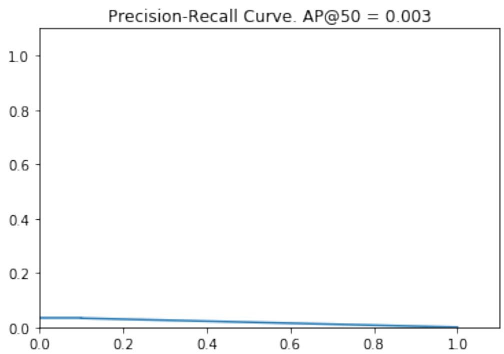

Figure 6: The precision-recall curve for the image in Figure 2.

Thus, the Mask R-CNN architecture was able to detect and segment the quasi-particles, as well as correctly classify the labeled classes, providing coherent results.

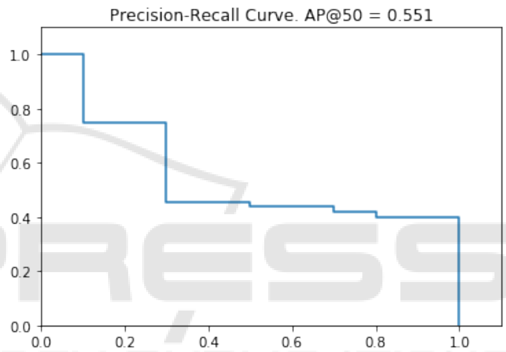

Figure 7: The precision-recall curve for the image in Figure 3.

6 CONCLUSION

In this work, we propose to obtain the quasi-particle size in an imaging method based on the implementation of the Mask R-CNN algorithm for the detection and segmentation of the quasi-particles according to the desired class. To do so, we label the dataset by classes according to the specified particle size range.

We performed four training sessions with hyperparameters adjusted and customized for the problem. The model evaluation demonstrated good detection and segmentation, correctly predicted classes, and well-defined quasi-particle edges. The model also had good results by avoiding the segmentation of overlapping and occluded particles, a factor that could lead to the wrong prediction of the class.

The mAP metric used in evaluating the Mask R-CNN model customized for this problem had results between 0.2333 and 0.2585 for an IoU of 0.5. In the individual evaluation of the AP metric of each image, we verified that the AP values were lower for images that contained many particles present in the sample and higher AP values for images that contained few particles present.

This factor may be associated with a small number of labels in the validation set (only 10 per image), increasing the probability for images with few particles that the predicted value was associated with labeled ground truth. For better AP results for these classes, we suggest in future work that a greater proportion of particles be labeled in the validation set and that the training and validation sets have particles from different classes labeled in the same image.

We emphasize that our implementation has the challenge of working with images derived from an industrial environment. These images are complex, as they present homogeneity in color, texture, complex background, overlapping, and occlusion. Furthermore, we did not find any database available for the implementation, and we designed our database.

From the results obtained in this step, it was possible to raise new hypotheses of approaches to improve the algorithm to obtain the particle size distribution of the quasi-particles present in a sample in future work. The development of applied solutions with deep learning can bring significant benefits, both in the improvement of processes and in the insertion of steelmaking processes in Industry 4.0.

REFERENCES

Bello, R.-W., Mohamed, A. S. A., and Talib, A. Z. (2021). Contour extraction of individual cattle from an image using enhanced mask r-cnn instance segmentation method. *IEEE Access*, 9:56984–57000.

Chen, D., Guo, D., Liu, S., and Liu, F. (2020). Microstructure instance segmentation from aluminum alloy metallographic image using different loss functions. *Symmetry*, 12(4):639.

Cohn, R., Anderson, I., Prost, T., Tiarks, J., White, E., and Holm, E. (2021). Instance segmentation for direct measurements of satellites in metal powders and automated microstructural characterization from image data. *JOM*, pages 1–14.

De Cesaro Júnior, T. et al. (2020). Insectcv: um sistema para detecção de insetos em imagens digitais.

Girshick, R. (2015). Fast r-cnn. In *Proceedings of the IEEE international conference on computer vision*, pages 1440–1448.

He, K., Gkioxari, G., Dollár, P., and Girshick, R. (2017). Mask r-cnn. In *Proceedings of the IEEE international conference on computer vision*, pages 2961–2969.

He, K., Zhang, X., Ren, S., and Sun, J. (2016). Deep residual learning for image recognition. In *Proceedings of the IEEE conference on computer vision and pattern recognition*, pages 770–778.

Johnson, J. W. (2018). Adapting mask-rcnn for automatic nucleus segmentation. *arXiv preprint arXiv:1805.00500*.

LeCun, Y., Bengio, Y., and Hinton, G. (2015). Deep learning. *nature*, 521(7553):436–444.

Long, J., Shelhamer, E., and Darrell, T. (2015). Fully convolutional networks for semantic segmentation. In *Proceedings of the IEEE conference on computer vision and pattern recognition*, pages 3431–3440.

Ren, S., He, K., Girshick, R., and Sun, J. (2015). Faster r-cnn: Towards real-time object detection with region proposal networks. *Advances in neural information processing systems*, 28:91–99.

Soloy, A., Turki, I., Fournier, M., Costa, S., Peuziat, B., and Lecoq, N. (2020). A deep learning-based method for quantifying and mapping the grain size on pebble beaches. *Remote Sensing*, 12(21):3659.

Tu, S., Yuan, W., Liang, Y., Wang, F., and Wan, H. (2021). Automatic detection and segmentation for group-housed pigs based on pigms r-cnn. *Sensors*, 21(9):3251.

Vuola, A. O., Akram, S. U., and Kannala, J. (2019). Mask-rcnn and u-net ensembled for nuclei segmentation. In *2019 IEEE 16th International Symposium on Biomedical Imaging (ISBI 2019)*, pages 208–212. IEEE.

Wu, Q., Feng, D., Cao, C., Zeng, X., Feng, Z., Wu, J., and Huang, Z. (2021). Improved mask r-cnn for aircraft detection in remote sensing images. *Sensors*, 21(8):2618.

Xi, D., Qin, Y., and Wang, Y. (2020). Vision measurement of gear pitting under different scenes by deep mask r-cnn. *Sensors*, 20(15):4298.

Xie, S., Girshick, R., Dollár, P., Tu, Z., and He, K. (2017). Aggregated residual transformations for deep neural networks. In *Proceedings of the IEEE conference on computer vision and pattern recognition*, pages 1492–1500.

Xu, B., Wang, W., Falzon, G., Kwan, P., Guo, L., Sun, Z., and Li, C. (2020). Livestock classification and counting in quadcopter aerial images using mask r-cnn. *International Journal of Remote Sensing*, 41(21):8121–8142.

Zhang, Q., Liu, Y., Gong, C., Chen, Y., and Yu, H. (2020). Applications of deep learning for dense scenes analysis in agriculture: A review. *Sensors*, 20(5):1520.

Zhang, R., Cheng, C., Zhao, X., and Li, X. (2019). Multiscale mask r-cnn–based lung tumor detection using pet imaging. *Molecular imaging*, 18:1536012119863531.

Zhao, K., Kang, J., Jung, J., and Sohn, G. (2018). Building extraction from satellite images using mask r-cnn with building boundary regularization. In *Proceedings of the IEEE Conference on Computer Vision and Pattern Recognition Workshops*, pages 247–251.